

Ferrodistorstive orbital ordering in the layered nickelate NaNiO_2 : A density-functional study

H. Meskine and S. Satpathy
(dated: April 14, 2024)

The electronic structure and magnetism in the sodium nickelate NaNiO_2 in the low-temperature phase is studied from density-functional calculations using the linear muffin-tin orbitals method. An antiferromagnetic solution with a magnetic moment of 0.7 μ_B per Ni ion is found. A ferrodistorstive orbital ordering is shown to occur due to the Jahn-Teller distortion around the Ni^{+3} ion in agreement with the orbital ordering inferred from neutron diffraction. While the intralayer exchange is ferromagnetic, the interlayer exchange is weakly antiferromagnetic, mediated by a long Ni-O-Na-O-Ni superexchange path.

Since their discovery in the early fifties¹, the nickelates have been the subject of attention due to their many applications such as the base materials in batteries. More recently, the family of compounds $\text{Li}_x\text{Me}_x\text{NiO}_2$ (Me being a metal) have attracted special interest due to their triangular lattice structure which makes them good candidates as frustrated magnetic systems. In fact, magnetic or orbital frustration mechanisms are usually invoked in explaining the unusual behavior of LiNiO_2 . Many different scenarios have been proposed to explain the absence of orbital and magnetic orderings in LiNiO_2 , such as spin-glass,² quantum disordered state,^{3,4} spin-orbital liquid,⁵ impurity effect,⁶ or frustrated anti-ferromagnet.⁷ In comparison, NaNiO_2 seems to show none of the unusual behaviors of its sister compound including the magnetic behavior.^{8,9} For example, while in LiNiO_2 , no long-range magnetic order has been observed, NaNiO_2 in contrast is a type A antiferromagnet (ferromagnetic layers stacked on top of one another and coupled antiferromagnetically). It has been a long puzzle as to why their magnetic properties are so different, in spite of the fact that the two compounds are very similar.

In this paper, we study the electronic structure of NaNiO_2 using density-functional methods, with the goal of gaining insight into the physics of this family of materials. The nature of orbital ordering as well as the origin of the magnetic exchange are also discussed.

The high-temperature hexagonal crystal structure of NaNiO_2 (space group $R\bar{3}m$, no. 166) is shown in Fig. 1. The compound undergoes a structural transition to a lower-symmetry monoclinic structure with the paramagnetic space group $C2/m$ (no. 12) at about 450 K, below which the oxygen octahedra become elongated. The magnetic transition is at a much lower temperature $T_N = 20\text{K}$ ⁹, below which the A-type antiferromagnetic structure occurs. The layered structure may be viewed as an arrangement of slightly elongated NiO_6 octahedra separated by Na sheets. In the low-temperature structure, the Jahn-Teller (JT) distortion leads to different Ni-O bond lengths: four short bonds of 1.91 Å and two long ones of 2.14 Å. The lattice parameters are listed in Table I. In the low-temperature phase, NaNiO_2 shows the ferro-distorstive orbital ordering caused by the Jahn-Teller distortions of the NiO_6 octahedra, which disap-

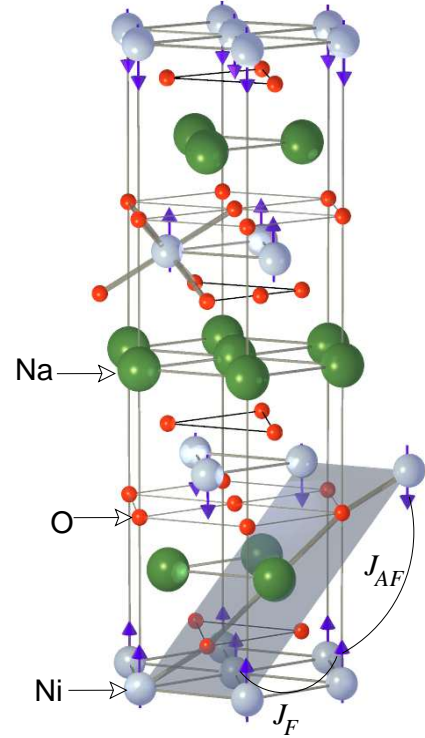


FIG. 1: High temperature crystal structure of NaNiO_2 . Calculations reported here are for the low-temperature phase ($C2/m$), but the high-temperature structure ($R\bar{3}m$) is shown here because it is simpler to visualize. The former is obtained by distorting the latter, including a Jahn-Teller stretching of the NiO_6 octahedra. The magnetic ordering is antiferromagnetic type A, with ferromagnetic interaction within the layer and antiferromagnetic interaction between the layers. The line connecting the Ni-O-Na-O-Ni atoms indicates the superexchange path and the rectangle joining the four Ni atoms has reference to the plane of the contour plot in Fig. 4.

pears in the high-temperature phase.

The band-structure calculations were performed for the low temperature structure using the local spin-density approximation (LSDA) to the density functional theory (DFT) as well as the $\backslash\text{LDA} + \text{U}\backslash$ approximation, using the linear muffin-tin orbitals (LMTO) method^{10,11}.

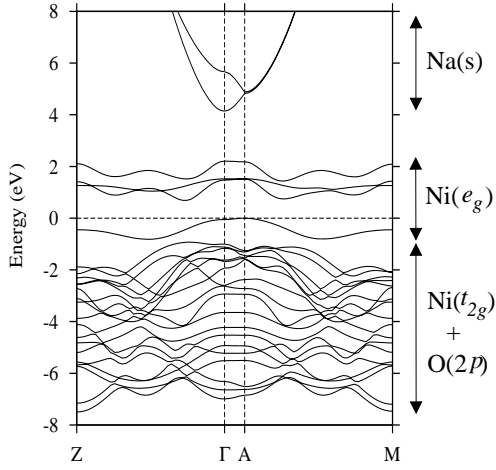


FIG. 2: Density-functional energy bands for the antiferromagnetic NaNiO_2 in the low-temperature structure obtained from the $\backslash\text{LDA}+U\backslash$ calculations. The unit cell has two formula units: $(\text{NaNiO}_2)_2$. The e_g bands are split near the Fermi level due to the Jahn-Teller and exchange interactions.

For the antiferromagnetic structure, the symmetry is not reduced further and the magnetic unit cell is also monoclinic with space group $C2/m$ with two formula units per unit cell. Within the LMTO atomic sphere approximation (LMTO-ASA), the antiferromagnetic (AF) type A structure was found to be the ground state, lower in energy than both the ferromagnetic (FM) and paramagnetic structures.

In the $\backslash\text{LDA}+U\backslash$ method,¹³ the Coulomb interactions between the localized electrons (Ni(d)) are subtracted from the LDA total energy and a "more proper" Hubbard-like term is added, so that the corrected energy functional reads:

$$E = E_{\text{LDA}} - U \sum_i (n_i - 1/2) + \sum_{i \neq j} \frac{U}{2} n_i n_j; \quad (1)$$

where N is the total number of the localized electrons, n_i is the occupancy of the i^{th} localized orbital, and U is the screened Coulomb energy. The orbital energies are obtained by taking the derivatives with respect to the orbital occupation, so that

$$\epsilon_i = \partial E / \partial n_i = \epsilon_{\text{LDA}} + U (1/2 - n_i); \quad (2)$$

Thus with respect to the LDA results, the energies of the occupied orbitals are shifted by $-U/2$, while those of the unoccupied states are shifted up by the amount $U/2$. In the actual calculations, one works with a slightly more complicated functional that includes properly the direct and the exchange Coulomb interactions, parameterized by the screened interactions U and J .

The band structure of NaNiO_2 in the AF-type A magnetic structure calculated with the $\backslash\text{LDA}+U\backslash$ method,

TABLE I: Atomic positions and sphere radii used in the LMTO calculations. Lattice parameters for the monoclinic unit cell (space group $C2/m$) are $a = 5.311 \text{ \AA}$, $b = 2.840 \text{ \AA}$, $c = 5.568 \text{ \AA}$, and $\beta = 110.44^\circ$ (Ref.⁹).

atom	x=a	y=b	z=c	S [Å]	site
Na	0	1/2	1/2	1.72	2d
Ni	0	0	0	1.28	2a
O	0.2832	0	0.804	1.04	4i

with $U = 5 \text{ eV}$ and $J = 0.5 \text{ eV}$, are shown in Fig. 2. While the LSDA results showed a metallic band structure because of a slight overlap between the bands derived from the $e_g^{(1)}$ and $e_g^{(2)}$ Ni(d) states at the same Ni site, the overlap disappears when the correlation effects are included within the $\backslash\text{LDA}+U\backslash$ formalism. Only a small value of U is needed to open up the gap, suggesting a robust insulating gap in the compound resulting from electronic correlation.

The bands indicate a low-spin state, with the t_{2g} states being completely occupied while the e_g states are only quarter-filled ($t_{2g}^6 e_g^1$). As indicated from the densities-of-states (Fig. 3), the t_{2g} and e_g bands are split by a strong crystal-field splitting, while the $e_g^{(1)}$ and $e_g^{(2)}$ are split by the exchange coupling by the amount $\Delta_{\text{ex}} = 0.7 \text{ eV}$. The Ni($e_g^{(1)}$) occupancy makes the system JT-active in the low-temperature phase, lifting the degeneracy of the e_g levels, with a JT energy of $\Delta_{\text{JT}} = 0.6 \text{ eV}$.

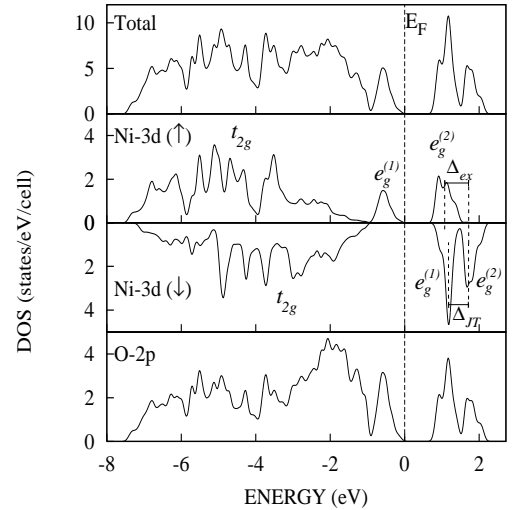


FIG. 3: Electronic Density of states for NaNiO_2 . Δ_{JT} and Δ_{ex} refer to the Jahn-Teller and the exchange splittings, respectively.

The calculated magnetic moment is $\mu = 0.51 \mu_B/\text{Mn}$ obtained from the LSDA, which increases to $0.71 \mu_B/\text{Mn}$ in the $\backslash\text{LDA}+U\backslash$ results, as in the latter, the slight overlap between the $e_g^{(1)}$ and $e_g^{(2)}$ disappears, increasing the occupancy of the spin-up states. This is lower than the

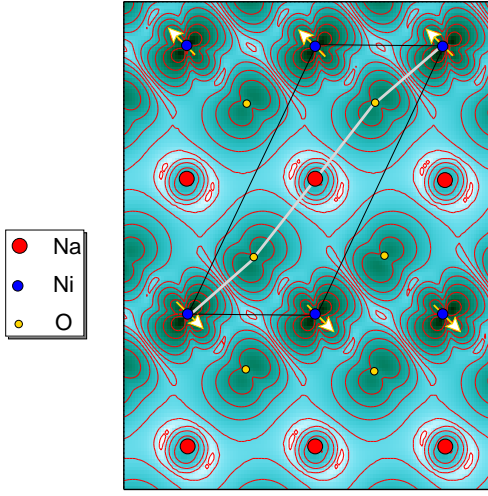


FIG. 4: (Color online) Charge density contours of the occupied Ni (d) bands (about 0.8 eV wide occurring just below E_F) showing the ferro-orbital ordering of the Ni (e_g) orbitals, as obtained from the LSDA calculations. The plane of the plot is the diagonal plane, defined by the rectangle drawn here and in Fig. 1. Arrows indicate the spins of the Ni^{3+} ions and the line joining the Ni-O-Na-O-Ni indicates the superexchange path. Contour values are given by $\rho_n = 0.10^n$, with $\rho_0 = 0.708 \text{ e/a}_0^3$, $\rho_1 = 0.575$, and $n = 0, \dots, 7$.

nominal magnetic moment of $1 \mu_B/\text{Ni}$ because of the strong hybridization between the O (2p) and the Ni (3d) states.

We have studied the orbital ordering by examining the occupancy of the various Mn (d) orbitals. In a frame of reference where the z axis points along the long Ni-O bond, we found the occupied Ni(d) electrons to be predominantly of $3z^2 - r^2$ character. The charge density contours for the occupied Mn (d) states, plotted in Fig. 4, shows the ferro-orbital ordering of the $3z^2 - r^2$ orbitals, with significant hybridization coming from the O (2p) states. Fig. 5 shows a sketch of the orbital order as obtained from the density-functional charge density. The charge density for the undistorted high temperature structure was also computed and we found no orbital order for that case.

The magnetic exchange interactions, the ferromagnetic J_F within the layer and the antiferromagnetic J_{AF} between the layers are both weak, with measured values being $J_F = 13 \text{ K}$ and $J_{AF} = 1 \text{ K}$.⁸ The exchange interactions are weak because the intralayer exchange involves a 90° Ni-O-Ni bond, while for the interlayer coupling, it is the long Ni-O-Na-O-Ni superexchange path that makes the exchange weak. The 90° Ni-O-Ni exchange within the layer has been examined in great detail in two recent papers^{14,15}.

For the exchange between the layers, we treat the Ni-O-Na hopping as an effective Ni-Na hopping between the Ni ($3z^2 - r^2$) and Na (s) orbitals on the Ni-O-Na-O-Ni superexchange path. The model Hamiltonian for the ef-

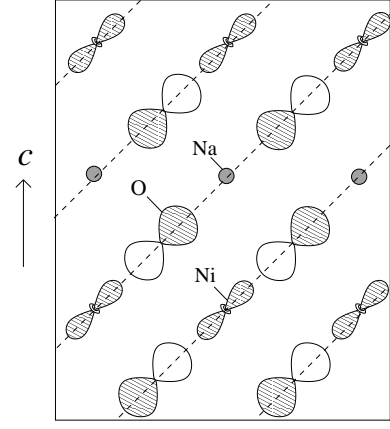


FIG. 5: Sketch of the orbital order in NaNiO_2 extracted from Fig. 4. The shaded lobes indicate a positive wave function, indicating the antibonding interaction between the Ni ($3z^2 - r^2$) and the O (p_z) orbitals.

fective Ni-Na-Ni path then reads

$$H_{\text{eff}} = \sum_{ij} t_{ij}^y c_i^\dagger c_j + \sum_i \epsilon_i n_i + \sum_i U_i n_i n_{i\uparrow}; \quad (3)$$

where t is the effective hopping between the Ni and the Na atoms, ϵ_i is the on-site energy, and the on-site Coulomb energies are U_d and U_s for the Ni (d) and the Na (s) orbitals, respectively.

The exchange interaction J_{AF} between Ni atoms is obtained by calculating the ground state of the Hamiltonian Eq. 3 for the ferromagnetic (FM) and antiferromagnetic (AF) configurations of the Ni ($e_g^{(1)}$) spins and then taking the difference: $J_{AF} = E_{\text{FM}} - E_{\text{AF}}$. For the FM case, we have two spin up electrons occupying the Na (s) and the Ni ($e_g^{(1)}$) states leading to a three-dimensional configuration space. Similarly, for the AF case, we have a 9×9 Hamiltonian (one spin up and one spin down electrons distributed among three orbitals of either spin, so that ${}^3C_1 - {}^3C_1 = 9$). The ground-state energies may be obtained by diagonalization of the Hamiltonians or by using the fourth order perturbation theory. The latter yields

$$J_{AF} = \frac{2t^4}{2\epsilon_{sd}} \frac{2}{U_s + 2\epsilon_{sd}} + \frac{1}{U_d}; \quad (4)$$

where ϵ_{sd} is the charge transfer energy from Ni (d) to Na (s). The first term is due to the exchange via the intermediate state with the two electrons on the Na atom, while the second is due to hopping between the two Ni orbitals via the Na atom. The exchange coupling is clearly antiferromagnetic. Taking typical values: $t \approx 0.3 \text{ eV}$, $\epsilon_{sd} \approx 5 \text{ eV}$, $U_d \approx 5 \text{ eV}$, and $U_s \approx 2 \text{ eV}$, the magnitude of the exchange is $J_{AF} \approx 0.1 \text{ meV}$, which is the right order of magnitude as compared to the experimental value of 1 K .

We thank Z.S. Popovic for valuable discussions and

acknowledge financial support by the U.S. Department of Energy under Contract No. DE-FG 02-00ER 45818.

-
- ¹ L.D. Dyer, D.S. Borie Jr., G.P. Smith, J. Am. Chem. Soc. 76, 1499 (1954).
 - ² A. Bapai and A. Banerjee, Phys. Rev. B 55, 12439 (1997).
 - ³ Y.Q. Li, M. Ma, D.N. Shi, and F.C. Zhang, Phys. Rev. Lett. 81, 3527 (1998).
 - ⁴ Y. Kitaoka, T. Kobayashi, A. Hoda, H. Wakabayashi, Y. Nino, H. Yamakage, S. Taguchi, K. Arita, M. Yamaura, K. Takano, A. Hirano, J. Phys. Soc. Jpn. 67, 3703 (1998).
 - ⁵ L.F. Feiner, A.M. Oleś, and J. Zaanen, Phys. Rev. Lett. 78, 2799 (1997).
 - ⁶ M.V. Mostovoy and D.I. Khomskii, Phys. Rev. Lett. 89, 227203 (2000).
 - ⁷ H. Yoshizawa, H. Mori, K. Hirota, and M. Ishikawa, J. Phys. Soc. Jpn. 59, 2631 (1990).
 - ⁸ E. Chappel, M.D. Núñez-Regueiro, F. Dupont, G. Chouteau, C. Darie, and A. Sulpice, Eur. Phys. J. B 17, 609 (2000).
 - ⁹ E. Chappel, M.D. Núñez-Regueiro, G. Chouteau, O. Isnard, and C. Darie, Eur. Phys. J. B 17, 615 (2000).
 - ¹⁰ O.K. Andersen and O. Jepsen, Phys. Rev. Lett. 53, 2571 (1984).
 - ¹¹ O.K. Andersen, Phys. Rev. B 12, 3060 (1975).
 - ¹² U. von Barth and L. Hedin, J. Phys. C 5, 1629 (1972).
 - ¹³ For example, see: V.I. Anisimov, F. Aryasetiawan, and A.I. Lichtenstein, J. Phys.: Condens. Matter 9, 767 (1997).
 - ¹⁴ M.V. Mostovoy and D.I. Khomskii, Phys. Rev. Lett. 89, 227203 (2002).
 - ¹⁵ A.M. Dare, R. Hayn, and J.-L. Richard, Europhys. Lett. 61, 803 (2003).